Biochemistry

Article

Cite This: *Biochemistry* 2019, 58, 3767−3776

pubs.acs.org/biochemistry

Conformational Dynamics of FERM-Mediated Autoinhibition in Pyk2 Tyrosine Kinase

Hanna S. Loving and Eric S. Underbakke*

Roy J. Carver Department of Biochemistry, Biophysics, and Molecular Biology, Iowa State University, Ames, Iowa 50011, United States

Supporting Information

ABSTRACT: Pyk2 is a non-receptor tyrosine kinase that evolved from gene duplication of focal adhesion kinase (FAK) and subsequent functional specialization in the brain and hemopoietic cells. Pyk2 shares a domain organization with FAK, with an N-terminal regulatory FERM domain adjoining the kinase domain. FAK regulation involves integrin-mediated membrane clustering to relieve autoinhibitory interactions between FERM and kinase domains. Pyk2 regulation remains cryptic, involving Ca^{2+} influx and protein scaffolding. While the mechanism of the FAK FERM domain in autoinhibition is well-established, the regulatory role of the Pyk2 FERM is ambiguous. We probed the mechanisms of FERM-mediated autoinhibition of Pyk2 using hydrogen/deuterium exchange mass spectrometry and kinase activity profiling. The results reveal FERM−kinase interfaces that are responsible for autoinhibition. Pyk2 autoinhibition impacts the activation loop conformation. In addition, the autoinhibitory FERM−kinase interface exhibits allosteric linkage with the FERM basic patch conserved in both FAK and Pyk2.

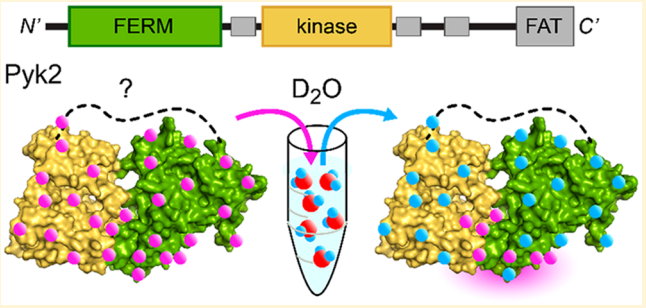

Proline-rich tyrosine kinase 2 (Pyk2, UniprotKB entry Q14289), also known as CAKβ, FAK2, or RAFTK, is a non-receptor tyrosine kinase and paralogue of focal adhesion kinase (FAK).[1] FAK is expressed ubiquitously, while Pyk2 is expressed in a limited number of cell types, primarily central nervous system (CNS) tissues and hematopoietic cells.[1−4] Pyk2 appears to have arisen in early chordates from a gene duplication of FAK, sharing 45% sequence identity (65% similarity).[5] As such, Pyk2 retains functional overlap with FAK and can compensate for some FAK functions in knockout models.[6−8] Nevertheless, Pyk2 function has specialized, adopting unique regulatory mechanisms and signaling roles.[9] Whereas FAK is localized primarily at focal adhesions, Pyk2 exhibits diffuse cytosolic localization.[6,10,11] FAK plays central signaling roles in cell adhesion, migration, proliferation, and embryonic development.[12,13] In contrast, Pyk2 is enriched in the postsynaptic density of neurons and serves to tune synaptic plasticity and regulate neuronal differentiation and migration in the CNS.[14−20] Pyk2 signaling is also involved in bone remodeling and leukocyte motility.[3,21] Canonical FAK activation involves recruitment to membrane focal adhesions via interactions with paxillin, talin, and vinculin at clustered integrins.[22−24] Strikingly, Pyk2 is activated by stimuli that elicit intracellular Ca^{2+} flux.[1,14,16,25] The marked differences in activation mechanisms between FAK and Pyk2 (i.e., integrin clustering vs Ca^{2+} flux) illustrate a common theme in cell signaling, repurposing of common domain components to respond to diverse stimuli. Understanding the molecular details of the divergent regulation of FAK and Pyk2 can illuminate how signaling diversity can arise through gene duplication and mechanistic shifts.

Pyk2 and FAK both exhibit a kinase domain flanked by a FERM (band 4.1/ezrin/radixin/moesin) domain at the N-terminus and a FAT (focal adhesion targeting) domain at the C-terminus (Figure 1). The FAT domain is tethered to the kinase

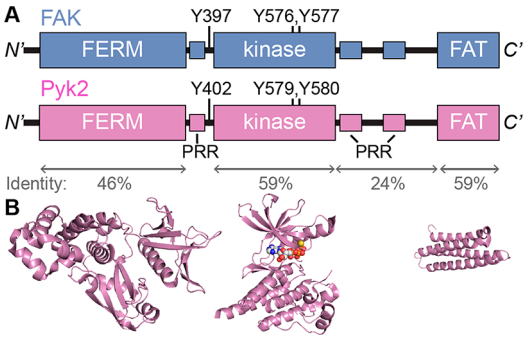

Figure 1. (A) Domain organization of Pyk2 and FAK. The pairwise identity of the *Homo sapiens* sequences, phosphorylated tyrosine residues, and proline-rich regions (PRR) are annotated. (B) Structural models of the Pyk2 domains from FERM (PDB entry 4eku), kinase (PDB entry 3fzp), and FAT (PDB entry 3gm2).[29,30]

Received: June 25, 2019
Revised: August 7, 2019
Published: August 12, 2019

DOI: 10.1021/acs.biochem.9b00541
Biochemistry 2019, 58, 3767−3776

via a putatively unstructured region containing several proline-rich regions. The multidomain architecture is punctuated by binding motifs, allowing Pyk2 and FAK to serve signaling roles as both a kinase and a scaffold.[22,26−28]

The mechanisms of FAK activation are not fully understood, but integrin-mediated clustering and membrane phosphoinositide interactions appear to relieve autoinhibitory interactions between the FERM and kinase domains.[24,31−34] The dimerization and clustering of derepressed FAK kinase domains allow for trans-autophosphorylation of residue Y397 in the FERM−kinase linker. The FAK linker phosphotyrosine serves as a docking site for Src kinase, leading to mutual phosphorylation of FAK and Src kinase domain activation loops (FAK residues Y576 and Y577). Ultimately, FAK clustering at the membrane of focal adhesions is responsible initiating the FAK signaling cascade.

The initial steps of Pyk2 activation remain unclear. Ca^{2+}-induced activation may involve dimerization via Ca^{2+}/calmodulin binding[35,36] or a Ca^{2+}-dependent multimerization via docking to the soluble scaffold protein PSD-95.[16] Nevertheless, downstream steps parallel those of FAK. Clustered Pyk2 autophosphorylates in trans at a FERM−kinase linker tyrosine (Y402), followed by Src binding and reciprocal activation loop phosphorylation for full activation.[37]

Clarifying the mechanism of Pyk2 autoinhibition is a prerequisite for understanding the activation mechanism. FAK autoinhibition is relatively well-defined by the X-ray crystallography-derived structure of an avian FAK construct encompassing the FERM-kinase domains (residues 31−686).[34] The FAK FERM-kinase structure revealed interactions between the kinase C-lobe and FERM F2 subdomain stabilizing a closed conformation. The closed conformation occludes the active site and sequesters the initial site of phosphorylation (Y397) far from the active site.

The autoinhibitory role of the Pyk2 FERM domain is not yet resolved.[9] To date, no structure of autoinhibited Pyk2 has been reported. Cell-based studies establish a clear regulatory role for the Pyk2 FERM.[11,38−41] Point mutations in the Pyk2 FERM domain can inhibit the activity of the kinase.[39] Expression of an autonomous Pyk2 FERM domain truncation inhibits the basal autophosphorylation of full-length Pyk2,[39,40,42] an observation echoed in FAK.[33] However, in some cases, Pyk2 FERM notably deviates from FAK FERM activity. Immunoprecipitation established that FAK FERM interacts with full-length FAK and the isolated FAK kinase domain, yet Pyk2 FERM exhibits negligible association with the dissociated Pyk2 kinase.[38,40] Intriguingly, FERM domain deletion strongly increases the level of FAK autophosphorylation,[33] yet FERM deletion in Pyk2 did not impact basal autophosphorylation in cells.[41]

To resolve the mechanism of Pyk2 autoinhibition, we probed functional interactions between FERM and kinase domains. Our approach integrates hydrogen/deuterium exchange mass spectrometry (HDX-MS) and site-directed mutagenesis to reveal inhibitory interfaces between the Pyk2 FERM and kinase domains. The investigation also informs on activation loop dynamics and allosteric coupling in the autoinhibited conformation.

MATERIALS AND METHODS

Plasmid Constructs. Plasmids used in the study were derived from the following sources. *Homo sapiens* Pyk2 [PTK2B (residues 1−1010)] was acquired from the Harvard PlasmID Repository (HsCD00022350). *H. sapiens* Pyk2 kinase domain expression vector PTK2BA encoding H_6-TEV-kinase (residues 414−692) was a gift from N. Burgess-Brown (Addgene, 42401). Cloning vector pET-H6-SUMO-TEV-LIC (1S) was a gift from S. Gradia (Addgene, 29659). The vector encoding *Yersinia pestis* YopH phosphatase (residues 1−468) was acquired from the Harvard PlasmID Repository (YpCD00017249). *Saccharomyces cerevisiae* SUMO protease H_6-Ulp1 (residues 423−621) expression vector pHYRS52 was a gift from H. Iwai (Addgene, 31122).

Expression vectors for Pyk2 domain truncations were generated using Gibson assembly.[43] Pyk2 FERM-kinase (residues 20−692) and FERM (residues 20−357) were assembled in frame with the His_6-SUMO solubility tag of pET-H6-SUMO-TEV-LIC (1S) to generate pHL001 and pHL002, respectively. Pyk2 FERM-kinase mutants were generated using the QuikChange (Agilent Genomics) site-directed mutagenesis strategy. All constructs were confirmed by DNA sequencing.

Protein Purification. Expression plasmids pHL001 and pHL002 encoding H_6-SUMO-FERM-kinase and H_6-SUMO-FERM, respectively, were transformed into Tuner(DE3) pLysS (Novagen) cells. Plasmid PTK2BA encoding H_6-TEV-kinase was transformed into BL21(DE3) cells. Starter cultures in LB medium supplemented with 50 μg/mL kanamycin were grown overnight at 37 °C. Four 1 L expression cultures of LB supplemented with 50 μg/mL kanamycin were inoculated (1:100) with the starter culture. Expression cultures were grown at 37 °C while being shaken to an OD_{600} of 0.35, at which point the temperature was decreased to 18 °C. At an OD_{600} of 0.5, the cells were induced with 1 mM isopropyl β-D-1-thiogalactopyranoside and incubated overnight at 18 °C while being shaken. Cells were harvested after 18 h by centrifugation at 3700*g* for 20 min. Cell pellets were stored at −80 °C until they were purified.

Harvested cells were thawed on ice with lysis buffer [150 mM NaCl, 50 mM HEPES, 15 mM imidazole, 1 mM phenylmethanesulfonyl fluoride, 20 mM EDTA, 5% glycerol, and 5 mM β-mercaptoethanol (βME) (pH 8)] supplemented with protease inhibitor cocktail II (Research Products International). Cells were lysed by six passages through an Emulsiflex-C3 homogenizer at 15000 psi. The lysate was cleared of cell debris by centrifugation at 20000*g* for 45 min at 4 °C. The cleared lysate was passed through a HisPur Ni-NTA Superflow agarose column (2 mL of resin, Thermo Scientific) pre-equilibrated in binding buffer [150 mM NaCl, 50 mM HEPES, 20 mM imidazole, 5% glycerol, and 5 mM βME (pH 8)]. The Ni-NTA column was washed with 15 column volumes of wash buffer [250 mM NaCl, 50 mM HEPES, 5% glycerol, 20 mM imidazole, and 5 mM βME (pH 8)]. His-tagged Pyk2 constructs were eluted with high-imidazole buffer [150 mM NaCl, 50 mM HEPES, 150 mM imidazole, 5% glycerol, and 5 mM β-ME (pH 8)]. Protein-containing elution fractions were dialyzed for 3 h with tag-specific protease, H_6-Ulp1 for SUMO-tagged constructs or H_6-TEV protease for the H_6-TEV-tagged kinase domain. Purification tags and proteases were removed by a subtractive second pass through the Ni-NTA column, re-equilibrated in binding buffer. Pyk2 constructs were further purified by gel filtration chromatography (GFC) using a Superdex 200 10/300 (GE Healthcare) column pre-equilibrated in GFC buffer [150 mM NaCl, 50 mM HEPES, 10% glycerol, and 1 mM DTT (pH 7.4)]. The purified proteins were concentrated using a Spin-X concentrator of 10K molecular weight cutoff PES (Corning). Concentrated proteins were aliquoted, snap-frozen in liquid N_2, and stored at −80 °C.

DOI: 10.1021/acs.biochem.9b00541
Biochemistry 2019, 58, 3767−3776

Kinase Assays. Kinase reactions were performed using a final concentration of 1 μM for each Pyk2 construct in a buffer consisting of 150 mM NaCl, 50 mM HEPES, 8 mM $MgCl_2$, 2 mM TCEP, 1 mM Na_3VO_4, and 10% glycerol (pH 7.4). Prior to the kinase reactions, the Pyk2 constructs were dephosphorylated with 0.1 μM H_6-YopH on ice for 30 min. Kinase reactions were initiated by addition of 1.6 mM ATP (final concentration). Reactions were quenched with sodium dodecyl sulfate−polyacrylamide gel electrophoresis (SDS−PAGE) loading dye followed by heat denaturation at 60 °C for 10 min. Phosphotyrosine production was assessed via anti-phosphotyrosine Western blotting. Briefly, autophosphorylation reaction mixtures were separated on SDS−PAGE gels and transferred to 0.2 μm nitrocellulose membranes at 25 V for 7 min using a Trans-Blot Turbo Transfer system (Bio-Rad). Membranes were blocked with BSA and incubated with the primary mouse anti-phosphotyrosine antibody (PY20, Thermo Scientific), followed by the goat anti-mouse HRP-conjugated secondary antibody (GOXMO HRP, Novex). Site-specific anti-phosphotyrosine blotting was performed with anti-phospho-PTK2B $pTyr^{402}$ (SAB4300173, Sigma) or anti-phospho-PYK2 $pTyr^{579}$, $pTyr^{580}$ (44-636G, Invitrogen) primary antibodies with the goat anti-rabbit HRP-conjugated secondary antibody (GOXRB HRP, Novex). Blots were imaged with an enhanced chemiluminescent substrate (Pierce).

Enzyme-coupled, continuous kinase assays were performed as previously described.[34,44] Purified Pyk2 variants were dephosphorylated by preincubation with 0.1 μM YopH for 30 min at 25 °C. Kinase activity was initiated by adding 0.5 mM ATP to reaction mixtures containing 1 μM Pyk2 FERM-kinase variant, Glu:Tyr (4:1) polypeptide substrate (Sigma), 0.28 mM NADH, 100 μM phosphoenolpyruvate, 100 units/mL lactate dehydrogenase, and 80 units/mL pyruvate kinase (Sigma) in a buffer consisting of 50 mM HEPES (pH 7.4), 150 mM NaCl, 8 mM $MgCl_2$, and 5% glycerol at 30 °C. NADH consumption was monitored at 340 nm with a Cary 60 ultraviolet−visible spectrophotometer (Agilent).

HDX-MS Mapping. Deuterium exchange reactions (27 uL) were initiated by diluting 50 pmol of Pyk2 constructs encompassing FERM, kinase, or FERM-kinase into D_2O buffer composed of final concentrations of 150 mM KCl, 50 mM HEPES, 2 mM DTT (pD 7.4), and 90% D_2O. Exchange reaction mixtures were incubated at 24 °C. At various time points (10 s, 45 s, 3 min, 10 min, 30 min, 1 h, 3 h, and 18 h), labeling reactions were quenched to pH 2.5 by addition of 4 M guanidinium chloride and 85 mM potassium phosphate (final concentrations) and snap-frozen in liquid N_2. Quenched exchange reaction mixtures were stored at −80 °C until LC-MS analysis. All exchange reactions were performed as three technical replicates.

For HDX-MS analysis, frozen exchange samples were quickly thawed and immediately injected (50 μL) into a temperature-controlled ACQUITY UPLC M-class HDX platform coupled in-line to an ESI-Q-TOF Synapt G2-Si instrument (Waters). Mobile phases consisted of solvents A (HPLC-grade aqueous 0.1% formic acid) and B (HPLC-grade acetonitrile and 0.1% formic acid). Samples were digested by flow through an in-line Enzymate BEH-immobilized pepsin column (5 μm particle, 300 Å pore, 2.1 mm × 30 mm; Waters) at 25 °C with a flow rate of 50 μL/min. Peptide products accumulated on an Acquity UPLC BEH C18 VanGuard trap column (1.7 μm, 130 Å, 2.1 mm × 5 mm; Waters) and desalted with 100% solvent A for 1.5 min at a flow rate of 120 μL/min. Peptides were subsequently resolved on an Acquity UPLC BEH C18 analytical column (1.7 μm, 130 Å, 1 mm × 100 mm; Waters) using a 7 min linear gradient from 6% to 35% solvent B. MS data were collected in positive ion, MS^E continuum, resolution mode with an m/z range of 50−2000. Ion mobility was used to further resolve peptides in the gas phase. Peptides were fragmented by argon gas collision for data-independent acquisition.

Pepsin-derived peptides were identified by fragmentation data using the ProteinLynx Global Server (PLGS version 3.0.3, Waters). The HDX data were analyzed with DynamX version 3.0 (Waters). Peptides identified by PLGS were manually curated after establishing thresholds of identifications in two of three unlabeled samples and 0.2 fragment per residue. Relative levels of deuterium incorporation for each peptide were calculated by DynamX after manual inspection of the spectra of each isotope envelope. Differences in deuterium incorporation between HDX treatments were assessed for representative time points approximating the actively exchanging regime of the time course. Statistical significance was determined using a two-tailed, unpaired t test. HDX-MS summary statistics are listed in Table S1 in accordance with community-based recommendations.[45]

Global HDX-MS was initiated by diluting Pyk2 FERM-kinase variants (120 pmol) into D_2O buffer composed of a final concentration of 150 mM KCl, 50 mM HEPES, 5 mM DTT (pD 7.4), and 87% D_2O. Exchange reaction mixtures were incubated at 21 °C. At various time points (30 s, 90 s, 3 min, and 30 min), labeling reactions were quenched to pH 2.5 by addition of 85 mM potassium phosphate (final concentration). Non-exchanged samples were acquired in matched H_2O buffers to establish intact mass baselines for each variant. Quenched samples were immediately injected (10 μL) into an ACQUITY UPLC H-class instrument coupled in line to an ESI-Q-TOF Synapt G2-Si instrument (Waters). Mobile phases consisted of solvents A (HPLC-grade aqueous 0.1% formic acid) and B (HPLC-grade acetonitrile and 0.1% formic acid). Exchange samples were desalted on a C4 column (5 μm, 1 mm × 50 mm; Restek) with 30% solvent B for 1 min at a flow rate of 400 μL/min. Intact protein was eluted with a rapid gradient ramp from 35% to 75% solvent B over 3 min. MS data were collected in positive ion, MS continuum, resolution mode with an m/z range of 300−4000. The intact mass of each exchange time point was deconvoluted from multiple charge states using the MaxEnt1 function of MassLynx (Waters).

RESULTS AND DISCUSSION

Given the well-established regulatory role of the FERM domain in FAK,[33,34] we tested whether the FERM domain is responsible for kinase autoinhibition in Pyk2. Accordingly, we compared autophosphorylation rates of purified Pyk2 truncations encompassing the FERM-kinase (residues 20−692) and the isolated kinase (residues 414−692). Both Pyk2 FERM-kinase and kinase constructs exhibited background tyrosine phosphorylation as purified from *Escherichia coli*, likely due to autophosphorylation induced by the high intracellular concentrations during overexpression.[37] Pyk2 constructs were dephosphorylated prior to kinase assays by pretreatment with YopH tyrosine phosphatase. Kinase activity time courses revealed that deletion of the FERM domain allows for a dramatically increased level of autophosphorylation of the Pyk2 kinase domain (Figure 2A and Figure S1). The FERM-kinase construct exhibits a considerably slower basal autophosphorylation rate. Western blotting with site-specific antibodies for

DOI: 10.1021/acs.biochem.9b00541
Biochemistry 2019, 58, 3767−3776

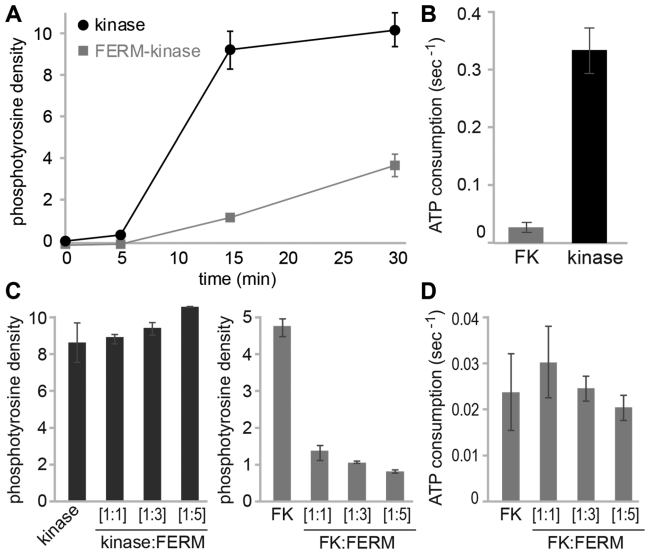

Figure 2. Pyk2 FERM domain inhibiting kinase autophosphorylation *in vitro*. (A) Kinase activity of Pyk2 kinase and FERM-kinase constructs (1 μM) was initiated by addition of ATP. Autophosphorylation was detected by Western blotting using the anti-phosphotyrosine antibody (PY20) and quantified by densitometry. (B) Kinase activity of Pyk2 FERM-kinase and kinase measured by ATP consumption using the Glu:Tyr (4:1) polypeptide substrate at 30 °C. ATP consumption was coupled to NADH oxidation with pyruvate kinase and lactate dehydrogenase in a continuous spectrophotometric assay monitoring absorbance at 340 nm for 5 min. (C and D) Relative activity of autonomous Pyk2 kinase or FERM−kinase (FK) preincubated with buffer or exogenous FERM (1, 3, or 5 μM). Kinase activity was assessed by monitoring either (C) autophosphorylation for 30 min at 25 °C via anti-phosphotyrosine Western blotting or (D) ATP consumption for 5 min at 30 °C via the enzyme-coupled assay, as in panel B. All error bars represent the standard deviation of three independent reactions. See Figure S1 for raw Western blotting data and loading controls.

Pyk2 phosphotyrosines confirmed that FERM-kinase autophosphorylation is predominantly localized to linker residue Y402 (Figure S2).

We also tested kinase activity using an enzyme-coupled, continuous spectrophotometric assay monitoring ADP product formation from phosphotransfer to an artificial exogenous peptide substrate (Figure 2B). The enzyme-coupled assay confirms that kinase activity, as measured by ATP consumption, is markedly higher (~14-fold) in the free kinase than in the FERM-kinase construct. Notably, our *E. coli*-derived Pyk2 FERM-kinase construct exhibits a basal specific activity (0.01−0.02 s^{-1}) comparable to the activity of the FAK FERM-kinase construct purified from insect cells (~0.005 s^{-1}), as measured by Lietha et al. using a similar assay.[34]

Next, we tested whether FERM-mediated inhibition of the Pyk2 kinase requires native intramolecular tethering. We tested the autophosphorylation activity of the isolated Pyk2 kinase incubated with the autonomous FERM domain (residues 20−357) added in trans at various stoichiometries (Figure 2C and Figure S1B). Addition of the autonomous FERM domain up to a 5-fold molar excess does not significantly inhibit Pyk2 kinase, suggesting that the regulatory interface between FERM and kinase requires the native linker for impactful affinity. In contrast, previous studies established that autonomous FAK FERM can inhibit the FAK kinase in trans.[33] Furthermore, addition of excess FAK FERM domain also suppresses the basal activity of the autoinhibited, full-length FAK.[33] To test whether Pyk2 FERM-kinase is sensitive to exogenous addition of the FERM domain, we tested FERM-kinase autophosphorylation with various stoichiometries of the added FERM domain. Indeed, the free FERM domain accentuates FERM-mediated kinase inhibition in the Pyk2 FERM-kinase construct (Figure 2C and Figure S1B). We were unable to detect a stable FERM:FERM-kinase complex by size exclusion chromatography. To investigate further, we tested whether the effect was evident using the enzyme-coupled kinase assay. Interestingly, exogenous FERM does not impact Pyk2 FERM-kinase activity when phosphotransfer to a peptide substrate is measured (Figure 2D). Given the difference in outcomes between autophosphorylation and peptide phosphorylation, it is possible that exogenous FERM transiently obscures the accessibility of the autophosphorylation substrate, linker residue Y402. Nevertheless, the mechanistic details and biological relevance of this exogenous FERM-mediated suppression of activity remain unclear for both FAK and Pyk2.

We sought to map interdomain interfaces that are responsible for FERM-mediated kinase inhibition in Pyk2. HDX-MS was used to compare the structural dynamics of Pyk2 FERM-kinase with the autonomous FERM or kinase domains. HDX-MS is a useful technique for studying protein folding, protein−protein interactions, allostery, and conformational dynamics.[46−50] HDX-MS measures the rates of backbone amide proton exchange to report on local chemical environments. H/D exchange rates are influenced by secondary structure, hydrogen bonding, dynamics, and solvent exposure. Increased rates of deuterium exchange result from disruptions in backbone hydrogen bonding, increased dynamics, or greater solvent accessibility. Decreased rates of exchange suggest local stabilization (e.g., formation of secondary structure and hydrogen bonding) or lower solvent accessibility. As such, exchange rate perturbations are valuable indicators of local protein dynamics, interfaces, and allostery.

We assessed the structural perturbations induced by the Pyk2 autoinhibitory FERM-kinase conformation by comparing H/D exchange rates with the free FERM and kinase domains. Changes in exchange rates were color-coded and mapped to the Pyk2 primary sequence (Figure 3A) and structural models of isolated FERM and kinase domains (Figure 3B). HDX-MS revealed several regions in both FERM and kinase impacted by the autoinhibited conformation.

The most striking suppressions of exchange rates of the autoinhibited Pyk2 FERM-kinase manifest at surfaces in the kinase C-lobe and FERM F2 subdomain (Figure 3B). The C-lobe and F2 subdomain surfaces are also the primary interface of the autoinhibited FAK FERM-kinase structure.[34] Indeed, alignment of Pyk2 kinase and FERM domain structures with the FAK FERM-kinase autoinhibited conformation reveals close agreement between the FAK interface and the Pyk2 exchange rate perturbations (Figure 4). The kinase exhibits the largest exchange rate decreases in the G helix (Figure 4, inset 4) and helix EF adjoining the activation loop (Figure 4, inset 5). The perturbations of the FERM F2 subdomain are smaller in magnitude and more diffuse (Figure 4, insets 2 and 6). Importantly, HDX-MS is highly sensitive to protein dynamics, and the perturbations may reflect conformational perturbations beyond the direct interface.

The autoinhibited conformation also impinges on the dynamics of the activation loop (Figure 4, inset 1). The activation loops of the autoinhibited FAK FERM-kinase and isolated Pyk2 kinase are not resolved in the crystallographically

DOI: 10.1021/acs.biochem.9b00541
Biochemistry 2019, 58, 3767−3776

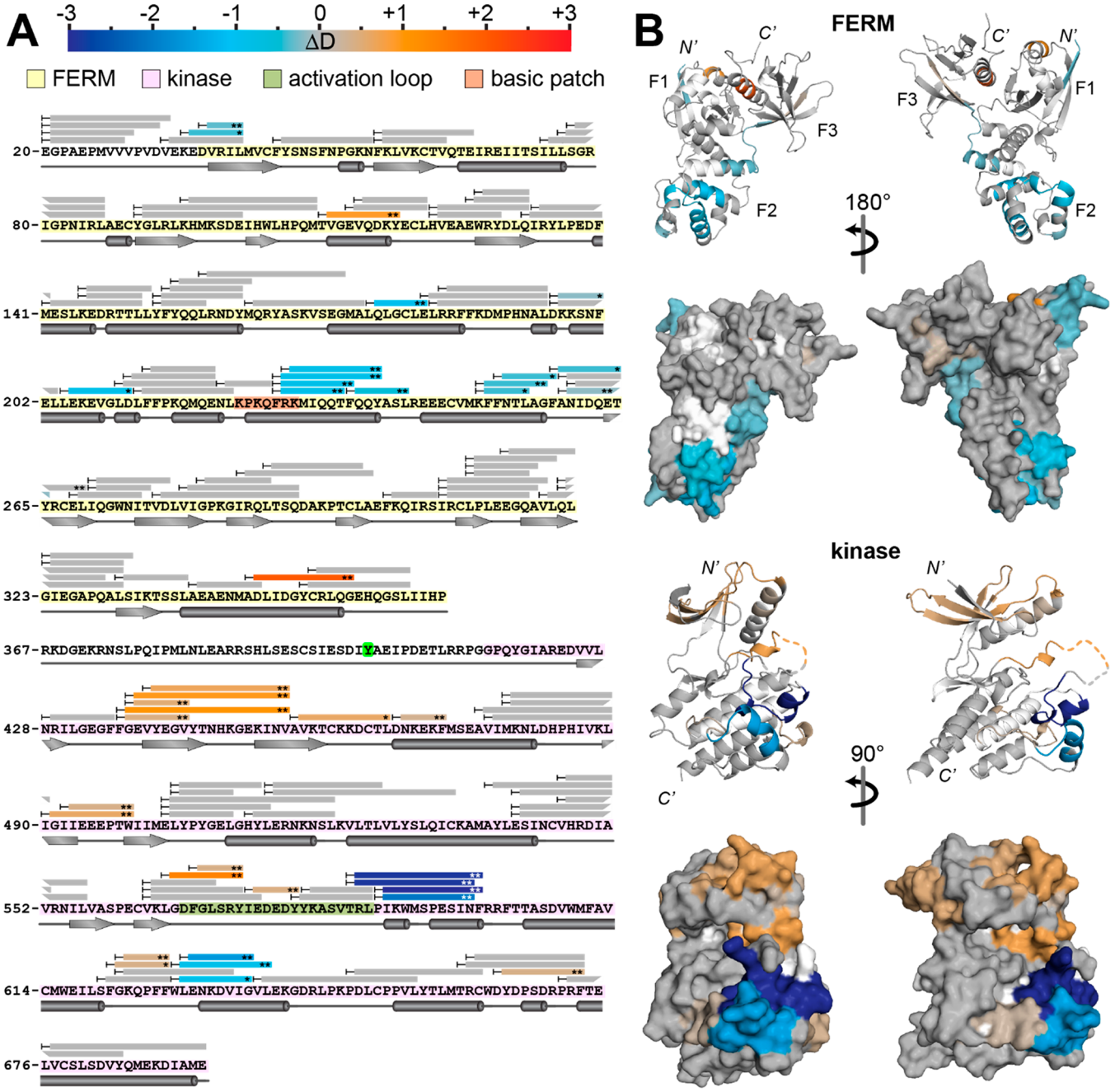

Figure 3. Comparison of HDX-MS exchange kinetics of Pyk2 FERM-kinase with autonomous FERM and kinase domains. (A) Peptide coverage is represented as bars mapped to primary sequence. Exchange rate perturbations are reported as the average difference in deuterium incorporation (ΔD) at time points approximating the midpoint of exchange. Peptides exhibiting significant exchange rate perturbations are color-coded according to the scale bar (top). Slower exchange in the FERM-kinase relative to autonomous FERM or kinase is reported in blue shades, while more rapid exchange in FERM-kinase is shown in red shades. Significance was assessed with a two-tailed, unpaired Student's t test ($*p < 0.005$; $**p < 0.001$). Peptides exhibiting negligible differences are colored gray. (B) Color-coded exchange rate perturbations were mapped to reported structures of the isolated Pyk2 FERM (PDB entry 4eku) and kinase (PDB entry 3cc6) domains. N′- and C′-termini and FERM subdomains (F1−F3) are annotated.

derived structure. Nevertheless, exchange rate suppression suggests that the autoinhibited conformation directly perturbs the accessibility or dynamics of the activation loop. Activation loop dynamics are likely to be critical to the regulation of both Pyk2 and FAK. For example, the phosphorylated FAK activation loop adopts a conformation sterically incompatible with the autoinhibited FERM−kinase interface.[34] Notably, we observe deprotection of the activation loop in the autoinhibited conformation. Because HDX is sensitive to multiple factors, we cannot definitively assign a mechanism for the observed exchange rate increase. Nevertheless, the FAK FERM-kinase structure may provide context. The FERM domain of autoinhibited FAK blocks access of the kinase to the activation loop, yet the loop remains relatively solvent accessible and unstructured,[34] consistent with the relatively rapid exchange observed in our HDX analysis. We speculate that dissociation of the FERM domain may allow for conformational rearrangement of the activation loop to form an element of semistabilized structure, manifesting as a suppression of exchange rates.

DOI: 10.1021/acs.biochem.9b00541
Biochemistry 2019, 58, 3767−3776

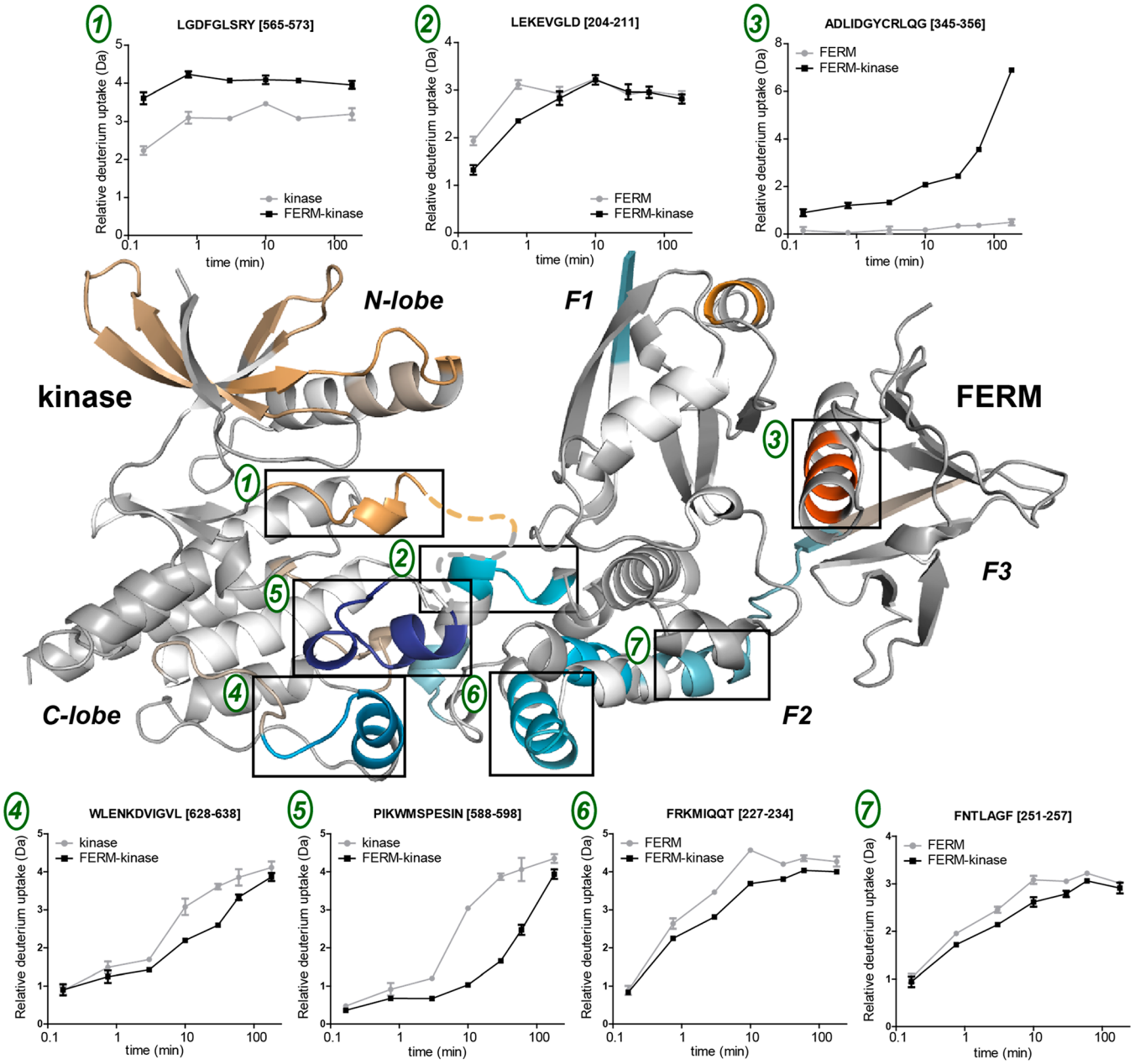

Figure 4. . HDX-MS exchange rate perturbations mapped to Pyk2 domains aligned in the autoinhibited conformation of the FAK FERM-kinase (PDB entry 2j0j). Representative deuterium uptake plots are shown for peptides derived from the featured, numbered regions. Error bars represent the standard deviation of three technical replicates.

Notably, the FERM domain perturbations in the autoinhibited conformation overlap and adjoin a basic patch conserved in both Pyk2 and FAK (Figure 4, inset 7). The basic patch is distinct from the FAK FERM−kinase interface, but this region has been implicated in FAK activation[38] via interactions with the c-Met receptor tyrosine kinase[51] membrane phosphoinositides,[32] and FAT domain.[31] The impact on the basic patch suggests allosteric communication between the direct FERM−kinase interface and this functionally important surface. Indeed, how activational stimuli release the autoinhibitory FERM−kinase interaction in either FAK or Pyk2 is currently unknown. Allosteric coupling between basic patch and interface may provide a mechanism for activation. On a related note, the core α-helix of the Pyk2 FERM F2 subdomain has been implicated in Ca^{2+}/calmodulin binding and activation of Pyk2.[35] HDX-MS reveals slight perturbations in this helix. However, the solvent accessibility of this helix is minimal, and it is unclear how calmodulin could access this proposed binding site.

Pyk2 FERM and kinase domains exhibit other exchange rate perturbations remote from the putative direct interface. There is faint evidence of perturbations in the FERM F1 subdomain and kinase N-lobe. These regions that make slight contacts with the FERM−kinase linker in the autoinhibited FAK structure.[34] The absence of this linker in the autonomous FERM and kinase constructs may be responsible for the effects in the N-lobe and F1 subdomain. In addition, one F3 subdomain helix exhibits exchange rate suppression in the autoinhibited conformation, a region distinctly distant from the F2 surfaces (Figure 4, inset 3). Intriguingly, this F3 helix forms an important basic binding cleft

DOI: 10.1021/acs.biochem.9b00541
Biochemistry 2019, 58, 3767−3776

for phosphoinositides and membrane protein tails in other FERM-containing proteins.[52,53] The basic residues are not preserved in FAK and Pyk2, having been substituted with acidic residues. Nevertheless, there may be allosteric linkage between the F3 subdomain and the apparent FERM−kinase interface.

While HDX-MS is exquisitely sensitive to the dynamics of the polypeptide backbone, parallel approaches are helpful for testing the functional importance of conformational perturbations. To validate the autoinhibitory conformation indicated by HDX-MS, we designed a panel of Pyk2 variants with putatively disruptive residue substitutions. We reasoned that disruption of the autoinhibitory conformation would lead to a de-repression of kinase activity. This approach serves as an orthogonal approach to HDX-MS, shifting from a focus on backbone conformational dynamics to the sensitivity of kinase activity to residue side chain disruption.

Eight Pyk2 FERM-kinase variants were generated and purified with residue substitutions engineered at surface sites within and outside the regions identified by HDX-MS (Figure 5A). F187A, E595R, and F599D were selected to probe the C-lobe−F2 subdomain interface observed in our Pyk2 HDX-MS analysis and the FAK FERM-kinase structure.[34] L58A and E404P were selected to test a feature of the FAK FERM-kinase conformation. In FAK, the initial site of autophosphorylation, linker residue Y397 is incorporated into a β-sheet in the F1 subdomain. We predicted that substitutions at the linker residue (E404P) and F1 β-strand (L58E) could disrupt formation of this possible feature of the autoinhibited conformation in Pyk2. Three residue substitutions (Y265A, L311A, and E342R) were also selected in the F3 subdomain. The F3 subdomain is distant from the autoinhibitory interface in FAK FERM-kinase, yet exchange rate perturbations appeared therein in Pyk2 FERM-kinase.

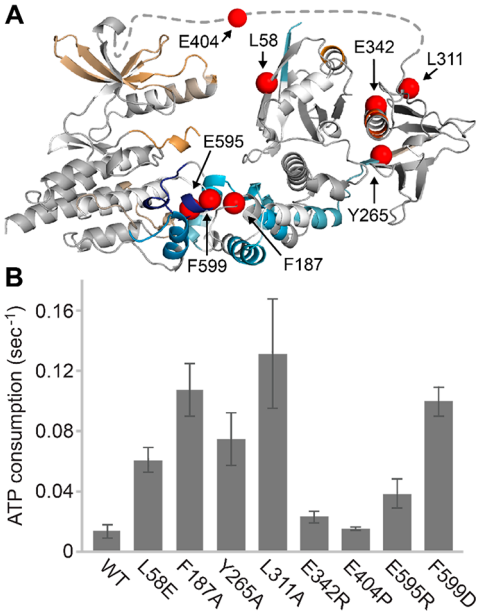

Figure 5. Kinase activity of Pyk2 FERM-kinase variants. (A) Residues selected for putatively disruptive mutations are highlighted as spheres on Pyk2 kinase and FERM domains with HDX-MS exchange rate perturbations mapped. The dotted line represents the FERM−kinase linker. (B) Kinase activity of each purified Pyk2 FERM-kinase variant measured by ATP consumption using the Glu:Tyr (4:1) polypeptide substrate at 30 °C. ATP consumption was coupled to NADH oxidation with pyruvate kinase and lactate dehydrogenase in a continuous spectrophotometric assay monitoring absorbance at 340 nm for 5 min. Error bars represent the standard deviation of six independent activity assays.

The kinase activity of the Pyk2 variants was measured using the enzyme-coupled, continuous spectrophotometric assay (Figure 5B). All variants were dephosphorylated with YopH prior to the assay. Several of the Pyk2 variants exhibited increased kinase activity, indicating a disruption or relaxation of the autoinhibited conformation. F599D and F187A exhibited striking increases in activity, consistent with the importance of the N-lobe−F2 subdomain interface in stabilizing the autoinhibited conformation. Indeed, an F596D FAK FERM-kinase variant, the residue homologous to Pyk2 F599D, exhibited a similar large increase (~7-fold) in kinase activity.[34] Nevertheless, E595R exhibited a marginal increase in activity, indicative of some tolerance for variation in the putative interface. Indeed, perturbations to conformational dynamics revealed by HDX-MS are not necessarily limited to the thermodynamically important core ("hot spot") of an interface, especially because HDX-MS monitors protein backbone dynamics rather than side chain interactions.

Of the residues designed to test the linker conformation, E404P was indistinguishable from wild-type (WT) basal activity. However, L58E exhibited a nearly 5-fold activation. Stable association of the linker with the FERM F1 subdomain may, indeed, play a role in Pyk2 autoinhibition. Alternatively, kinase N-lobe−FERM F1 subdomain contacts may stabilize autoinhibition. However, HDX-MS analysis reports negligible perturbations in this region, and the FAK FERM-kinase structure revealed proximity but little direct contact.[34]

Surprisingly, two F3 subdomain variants demonstrated Pyk2 activation. Both Y265A and L311A activated the Pyk2 kinase >5-fold higher than the basal WT activity. E342R was not stimulatory. Interestingly, the strongly activating L311A substitution is adjacent to a Pyk2 residue investigated previously, I308E.[39] In transfected glioma cells, I308E abolishes Pyk2 autophosphorylation. Assuming that the Pyk2 autoinhibitory interface is primarily mediated by F2−C-lobe contacts, the F3 subdomain is likely quite distant from the direct kinase interface. The sensitivity of F3 to mutation and kinase-dependent exchange rate perturbation indicates allosteric linkage between F2 and F3 surfaces of the FERM domain.

We hypothesize that Pyk2 FERM-kinase variants exhibiting kinase activation disrupt the inhibitory interface, shifting the equilibrium toward an open, FERM-dissociated conformation. We were especially interested in whether the putatively allosteric variants (Y265A and L311A) activated the kinase by influencing the global conformation. To test the extent of the conformational impact of the activation Pyk2 FERM-kinase variants, we employed global HDX-MS to monitor the general uptake of deuterium throughout the intact protein. WT, F187A, F599D, Y265A, and L311A variants of Pyk2 FERM-kinase were subjected to D_2O exchange for various time points, quenched, and quickly analyzed for intact mass shifts as deuterium accumulated.

To varying degrees, all activational Pyk2 variants exhibited modest increases in global exchange rates (Figure 6). Throughout the measured exchange time course, variants directly involved in the putative inhibitory interface (F187A and F599D) exhibited the largest magnitude increases in deuterium accumulation (20−40 Da), relative to that of the WT. The putatively allosteric variants (Y265A and L311A) also showed slightly increased rates of global exchange, ranging from

DOI: 10.1021/acs.biochem.9b00541
Biochemistry 2019, 58, 3767−3776

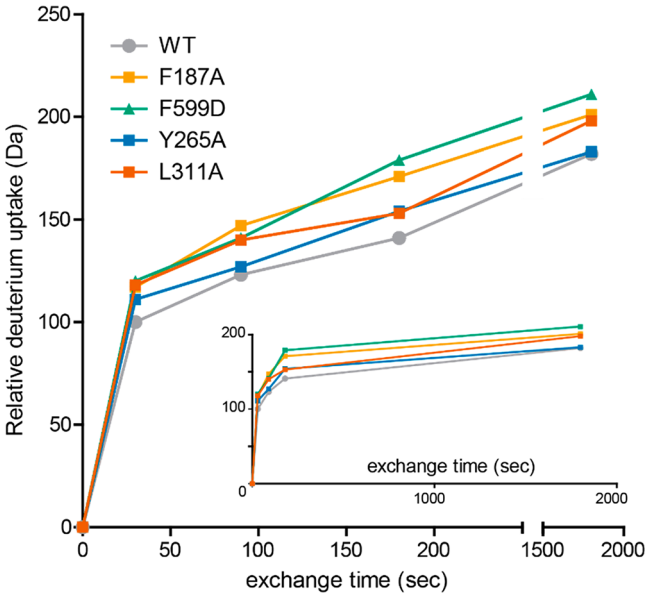

Figure 6. Activational variants of Pyk2 FERM-kinase exhibit increased global deuterium exchange. Deuterium uptake was calculated relative to the non-exchanged (0 s) intact mass of each variant. The theoretical maximal deuterium uptake is 545 Da, corrected for the D_2O content of exchange reactions. The exchange time axis is segmented to show early points (0–250 s) and the final point (1800 s). The inset shows the global deuterium uptake of each variant plotted with an unsegmented, linear time axis.

4 to 20 Da throughout the time course. Notably, all variants plateau toward a slower kinetic regime after the first 3 min, indicative of a similarly exchange-resistant, well-folded domain core (Figure 6, inset). An increased rate of global exchange is consistent with deprotection of an autoinhibitory interface in activating variants. However, we cannot rule out additional factors, such as localized increases in surface dynamics that could impact the kinase activity.

Taken together, HDX-MS analysis and activity profiling confirm that FERM domain interaction with the kinase is responsible for Pyk2 autoinhibition. Mapping of the interface suggests an autoinhibitory Pyk2 conformation compatible with the FAK conformation. However, HDX-MS revealed impacts on conformational dynamics distinct from the putative interface, including the functionally important basic patch. In addition, Pyk2 variants designed to disrupt local structure demonstrate that Pyk2 is sensitive to activation by perturbations in all three FERM subdomains. The apparent allosteric communication may confer a mechanism for communicating stimulatory Ca^{2+}/calmodulin binding with release of the Pyk2 autoinhibitory interface. It is also possible that allosteric communication can sensitize Pyk2 to regulatory protein interactions and post-translational modifications. We surmise that the allosteric communication between various FERM surfaces and the kinase interface may also be functionally relevant to the activation of FAK and other FERM proteins.

■ ASSOCIATED CONTENT

Supporting Information

The Supporting Information is available free of charge on the ACS Publications website at DOI: 10.1021/acs.biochem.9b00541.

Pyk2 FERM-kinase and kinase autophosphorylation Western blots (Figure S1), Pyk2 FERM-kinase site-specific autophosphorylation (Figure S2), and a summary of HDX-MS data (Table S1) (PDF)

Exported HDX state data for FERM-kinase versus FERM (Table S2) and exported HDX state data for FERM-kinase versus kinase (Table S3) (XLSX)

Accession Codes

Proline-rich tyrosine kinase 2 (Pyk2), UniprotKB Q14289.

■ AUTHOR INFORMATION

Corresponding Author

*E-mail: esu@iastate.edu.

ORCID

Eric S. Underbakke: 0000-0003-4269-7339

Funding

This work was supported by Grant 1715411 from the National Science Foundation, Division of Molecular and Cellular Biosciences.

Notes

The authors declare no competing financial interest.

■ ACKNOWLEDGMENTS

LC-MS/MS instrument acquisition was supported by a gift from the Roy J. Carver Charitable Trust. The authors thank Graciela Gautier for experimental assistance.

■ ABBREVIATIONS

HDX-MS, hydrogen/deuterium exchange mass spectrometry; FERM, band 4.1/ezrin/radixin/moesin; PDB, Protein Data Bank.

■ REFERENCES

(1) Lev, S., Moreno, H., Martinez, R., Canoll, P., Peles, E., Musacchio, J. M., Plowman, G. D., Rudy, B., and Schlessinger, J. (1995) Protein tyrosine kinase PYK2 involved in Ca^{2+}-induced regulation of ion channel and MAP kinase functions. *Nature 376*, 737–745.

(2) Avraham, S., London, R., Fu, Y., Ota, S., Hiregowdara, D., Li, J., Jiang, S., Pasztor, L. M., White, R. A., Groopman, J. E., and Avraham, H. (1995) Identification and characterization of a novel related adhesion focal tyrosine kinase (RAFTK) from megakaryocytes and brain. *J. Biol. Chem. 270*, 27742–27751.

(3) Okigaki, M., Davis, C., Falasca, M., Harroch, S., Felsenfeld, D. P., Sheetz, M. P., and Schlessinger, J. (2003) Pyk2 regulates multiple signaling events crucial for macrophage morphology and migration. *Proc. Natl. Acad. Sci. U. S. A. 100*, 10740–10745.

(4) Ostergaard, H. L., and Lysechko, T. L. (2005) Focal adhesion kinase-related protein tyrosine kinase Pyk2 in T-cell activation and function. *Immunol. Res. 31*, 267–281.

(5) Corsi, J.-M., Rouer, E., Girault, J.-A., and Enslen, H. (2006) Organization and post-transcriptional processing of focal adhesion kinase gene. *BMC Genomics 7*, 198.

(6) Sieg, D. J., Ilić, D., Jones, K., Damsky, C. H., Hunter, T., and Schlaepfer, D. D. (1998) Pyk2 and Src-family protein-tyrosine kinases compensate for the loss of FAK in fibronectin-stimulated signaling events but Pyk2 does not fully function to enhance FAK- cell migration. *EMBO J. 17*, 5933–5947.

(7) Fan, H., and Guan, J.-L. (2011) Compensatory function of Pyk2 protein in the promotion of focal adhesion kinase (FAK)-null mammary cancer stem cell tumorigenicity and metastatic activity. *J. Biol. Chem. 286*, 18573–18582.

(8) Verma, N., Keinan, O., Selitrennik, M., Karn, T., Filipits, M., and Lev, S. (2015) PYK2 sustains endosomal-derived receptor signalling

DOI: 10.1021/acs.biochem.9b00541
Biochemistry 2019, 58, 3767–3776

and enhances epithelial-to-mesenchymal transition. *Nat. Commun. 6*, 6064.
(9) Naser, R., Aldehaiman, A., Díaz-Galicia, E., and Arold, S. T. (2018) Endogenous control mechanisms of FAK and PYK2 and their relevance to cancer development. *Cancers 10*, 196.
(10) Schaller, M. D., and Sasaki, T. (1997) Differential signaling by the focal adhesion kinase and cell adhesion kinase *β*. *J. Biol. Chem. 272*, 25319−25325.
(11) Dunty, J. M., and Schaller, M. D. (2002) The N termini of focal adhesion kinase family members regulate substrate phosphorylation, localization, and cell morphology. *J. Biol. Chem. 277*, 45644−45654.
(12) Kleinschmidt, E. G., and Schlaepfer, D. D. (2017) Focal adhesion kinase signaling in unexpected places. *Curr. Opin. Cell Biol. 45*, 24−30.
(13) Schaller, M. D. (2010) Cellular functions of FAK kinases: insight into molecular mechanisms and novel functions. *J. Cell Sci. 123*, 1007−1013.
(14) Park, S.-Y., Avraham, H., and Avraham, S. (2000) Characterization of the tyrosine kinases RAFTK/Pyk2 and FAK in nerve growth factor-induced neuronal differentiation. *J. Biol. Chem. 275*, 19768−19777.
(15) Huang, Y.-Q., Lu, W.-Y., Ali, D. W., Pelkey, K. A., Pitcher, G. M., Lu, Y. M., Aoto, H., Roder, J. C., Sasaki, T., Salter, M. W., and MacDonald, J. F. (2001) CAK*β*/Pyk2 kinase is a signaling link for induction of long-term potentiation in CA1 hippocampus. *Neuron 29*, 485−496.
(16) Bartos, J. A., Ulrich, J. D., Li, H., Beazely, M. A., Chen, Y., Macdonald, J. F., and Hell, J. W. (2010) Postsynaptic clustering and activation of Pyk2 by PSD-95. *J. Neurosci. 30*, 449−463.
(17) Hsin, H., Kim, M. J., Wang, C. F., and Sheng, M. (2010) Proline-rich tyrosine kinase 2 regulates hippocampal long-term depression. *J. Neurosci. 30*, 11983−11993.
(18) Ivankovic-Dikic, I., Grönroos, E., Blaukat, A., Barth, B.-U., and Dikic, I. (2000) Pyk2 and FAK regulate neurite outgrowth induced by growth factors and integrins. *Nat. Cell Biol. 2*, 574−581.
(19) Fan, L., Lu, Y., Shen, X., Shao, H., Suo, L., and Wu, Q. (2018) Alpha protocadherins and Pyk2 kinase regulate cortical neuron migration and cytoskeletal dynamics via Rac1 GTPase and WAVE complex in mice. *eLife 7*, e35242.
(20) Giralt, A., Brito, V., Chevy, Q., Simonnet, C., Otsu, Y., Cifuentes-Díaz, C., de Pins, B., Coura, R., Alberch, J., Ginés, S., Poncer, J.-C., and Girault, J.-A. (2017) Pyk2 modulates hippocampal excitatory synapses and contributes to cognitive deficits in a Huntington's disease model. *Nat. Commun. 8*, 15592.
(21) Gil-Henn, H., Destaing, O., Sims, N. A., Aoki, K., Alles, N., Neff, L., Sanjay, A., Bruzzaniti, A., De Camilli, P., Baron, R., and Schlessinger, J. (2007) Defective microtubule-dependent podosome organization in osteoclasts leads to increased bone density in Pyk2−/− mice. *J. Cell Biol. 178*, 1053−1064.
(22) Arold, S. T. (2011) How focal adhesion kinase achieves regulation by linking ligand binding, localization and action. *Curr. Opin. Struct. Biol. 21*, 808−813.
(23) Mitra, S. K., and Schlaepfer, D. D. (2006) Integrin-regulated FAK-Src signaling in normal and cancer cells. *Curr. Opin. Cell Biol. 18*, 516−523.
(24) Goñi, G. M., Epifano, C., Boskovic, J., Camacho-Artacho, M., Zhou, J., Bronowska, A., Martín, M. T., Eck, M. J., Kremer, L., Gräter, F., Gervasio, F. L., Perez-Moreno, M., and Lietha, D. (2014) Phosphatidylinositol 4,5-bisphosphate triggers activation of focal adhesion kinase by inducing clustering and conformational changes. *Proc. Natl. Acad. Sci. U. S. A. 111*, E3177−E3186.
(25) Avraham, H., Park, S.-Y., Schinkmann, K., and Avraham, S. (2000) RAFTK/Pyk2-mediated cellular signalling. *Cell. Signalling 12*, 123−133.
(26) Chapman, N. M., Yoder, A. N., and Houtman, J. C. (2012) Non-catalytic functions of Pyk2 and Fyn regulate late stage adhesion in human T cells. *PLoS One 7*, No. e53011.
(27) Corsi, J.-M., Houbron, C., Billuart, P., Brunet, I., Bouvrée, K., Eichmann, A., Girault, J.-A., and Enslen, H. (2009) Autophosphorylation-independent and-dependent functions of focal adhesion kinase during development. *J. Biol. Chem. 284*, 34769−34776.
(28) Frame, M. C., Patel, H., Serrels, B., Lietha, D., and Eck, M. J. (2010) The FERM domain: organizing the structure and function of FAK. *Nat. Rev. Mol. Cell Biol. 11*, 802−814.
(29) Han, S., Mistry, A., Chang, J. S., Cunningham, D., Griffor, M., Bonnette, P. C., Wang, H., Chrunyk, B. A., Aspnes, G. E., Walker, D. P., Brosius, A. D., and Buckbinder, L. (2009) Structural characterization of proline-rich tyrosine kinase 2 (PYK2) reveals a unique (DFG-out) conformation and enables inhibitor design. *J. Biol. Chem. 284*, 13193−13201.
(30) Lulo, J., Yuzawa, S., and Schlessinger, J. (2009) Crystal structures of free and ligand-bound focal adhesion targeting domain of Pyk2. *Biochem. Biophys. Res. Commun. 383*, 347−352.
(31) Brami-Cherrier, K., Gervasi, N., Arsenieva, D., Walkiewicz, K., Boutterin, M. C., Ortega, A., Leonard, P. G., Seantier, B., Gasmi, L., Bouceba, T., Kadare, G., Girault, J. A., and Arold, S. T. (2014) FAK dimerization controls its kinase-dependent functions at focal adhesions. *EMBO J. 33*, 356−370.
(32) Cai, X., Lietha, D., Ceccarelli, D. F., Karginov, A. V., Rajfur, Z., Jacobson, K., Hahn, K. M., Eck, M. J., and Schaller, M. D. (2008) Spatial and temporal regulation of focal adhesion kinase activity in living cells. *Mol. Cell. Biol. 28*, 201−214.
(33) Cooper, L. A., Shen, T. L., and Guan, J. L. (2003) Regulation of focal adhesion kinase by its amino-terminal domain through an autoinhibitory interaction. *Mol. Cell. Biol. 23*, 8030−8041.
(34) Lietha, D., Cai, X., Ceccarelli, D. F. J., Li, Y., Schaller, M. D., and Eck, M. J. (2007) Structural basis for the autoinhibition of focal adhesion kinase. *Cell 129*, 1177−1187.
(35) Kohno, T., Matsuda, E., Sasaki, H., and Sasaki, T. (2008) Protein-tyrosine kinase CAK*β*/PYK2 is activated by binding Ca^{2+}/calmodulin to FERM F2 F2 helix and thus forming its dimer. *Biochem. J. 410*, 513−523.
(36) Xie, J., Allen, K. H., Marguet, A., Berghorn, K. A., Bliss, S. P., Navratil, A. M., Guan, J. L., and Roberson, M. S. (2008) Analysis of the calcium-dependent regulation of proline-rich tyrosine kinase 2 by gonadotropin-releasing hormone. *Mol. Endocrinol. 22*, 2322−2335.
(37) Park, S.-Y., Avraham, H. K., and Avraham, S. (2004) RAFTK/Pyk2 activation is mediated by trans-acting autophosphorylation in a Src-independent manner. *J. Biol. Chem. 279*, 33315−33322.
(38) Dunty, J. M., Gabarra-Niecko, V., King, M. L., Ceccarelli, D. F. J., Eck, M. J., and Schaller, M. D. (2004) FERM domain interaction promotes FAK signaling. *Mol. Cell. Biol. 24*, 5353−5368.
(39) Lipinski, C. A., Tran, N. L., Dooley, A., Pang, Y.-P., Rohl, C., Kloss, J., Yang, Z., McDonough, W., Craig, D., Berens, M. E., and Loftus, J. C. (2006) Critical role of the FERM domain in Pyk2 stimulated glioma cell migration. *Biochem. Biophys. Res. Commun. 349*, 939−947.
(40) Riggs, D., Yang, Z., Kloss, J., and Loftus, J. C. (2011) The Pyk2 FERM regulates Pyk2 complex formation and phosphorylation. *Cell. Signalling 23*, 288−296.
(41) Wu, S. S., Jácamo, R. O., Vong, S. K., and Rozengurt, E. (2006) Differential regulation of Pyk2 phosphorylation at Tyr-402 and Tyr-580 in intestinal epithelial cells: Roles of calcium, Src, Rho kinase, and the cytoskeleton. *Cell. Signalling 18*, 1932−1940.
(42) Lipinski, C. A., Tran, N. L., Menashi, E., Rohl, C., Kloss, J., Bay, R. C., Berens, M. E., and Loftus, J. C. (2005) The tyrosine kinase Pyk2 promotes migration and invasion of glioma cells. *Neoplasia 7*, 435−445.
(43) Gibson, D. G., Young, L., Chuang, R.-Y., Venter, J. C., Hutchison, C. A., III, and Smith, H. O. (2009) Enzymatic assembly of DNA molecules up to several hundred kilobases. *Nat. Methods 6*, 343−345.
(44) Schindler, T., Bornmann, W., Pellicena, P., Miller, W. T., Clarkson, B., and Kuriyan, J. (2000) Structural mechanism for STI-571 inhibition of abelson tyrosine kinase. *Science 289*, 1938−1942.
(45) Masson, G. R., Burke, J. E., Ahn, N. G., Anand, G. S., Borchers, C., Brier, S., Bou-Assaf, G. M., Engen, J. R., Englander, S. W., Faber, J., Garlish, R., Griffin, P. R., Gross, M. L., Guttman, M., Hamuro, Y., Heck, A. J. R., Houde, D., Iacob, R. E., Jørgensen, T. J. D., Kaltashov, I. A., Klinman, J. P., Konermann, L., Man, P., Mayne, L., Pascal, B. D.,

DOI: 10.1021/acs.biochem.9b00541
Biochemistry 2019, 58, 3767−3776

Reichmann, D., Skehel, M., Snijder, J., Strutzenberg, T. S., Underbakke, E. S., Wagner, C., Wales, T. E., Walters, B. T., Weis, D. D., Wilson, D. J., Wintrode, P. L., Zhang, Z., Zheng, J., Schriemer, D. C., and Rand, K. D. (2019) Recommendations for performing, interpreting and reporting hydrogen deuterium exchange mass spectrometry (HDX-MS) experiments. *Nat. Methods 16*, 595−602.

(46) Moroco, J. A., Alvarado, J. J., Staudt, R. P., Shi, H., Wales, T. E., Smithgall, T. E., and Engen, J. R. (2018) Remodeling of HIV-1 Nef Structure by Src-Family Kinase Binding. *J. Mol. Biol. 430*, 310−321.

(47) Offenbacher, A. R., Iavarone, A. T., and Klinman, J. P. (2018) Hydrogen-deuterium exchange reveals long-range dynamical allostery in soybean lipoxygenase. *J. Biol. Chem. 293*, 1138−1148.

(48) Hanson, Q. M., Carley, J. R., Gilbreath, T. J., Smith, B. C., and Underbakke, E. S. (2018) Calmodulin-induced conformational control and allostery underlying neuronal nitric oxide synthase activation. *J. Mol. Biol. 430*, 935−947.

(49) Knox, R., Lento, C., and Wilson, D. J. (2018) Mapping Conformational Dynamics to Individual Steps in the TEM-1 β-Lactamase Catalytic Mechanism. *J. Mol. Biol. 430*, 3311−3322.

(50) Zheng, J., Chang, M. R., Stites, R. E., Wang, Y., Bruning, J. B., Pascal, B. D., Novick, S. J., Garcia-Ordonez, R. D., Stayrook, K. R., Chalmers, M. J., Dodge, J. A., and Griffin, P. R. (2017) HDX reveals the conformational dynamics of DNA sequence specific VDR co-activator interactions. *Nat. Commun. 8*, 923.

(51) Chen, S. Y., and Chen, H. C. (2006) Direct interaction of focal adhesion kinase (FAK) with Met is required for FAK to promote hepatocyte growth factor-induced cell invasion. *Mol. Cell. Biol. 26*, 5155−5167.

(52) Hamada, K., Shimizu, T., Matsui, T., Tsukita, S., Tsukita, S., and Hakoshima, T. (2000) Structural basis of the membrane-targeting and unmasking mechanisms of the radixin FERM domain. *EMBO J. 19*, 4449−4462.

(53) Hamada, K., Shimizu, T., Yonemura, S., Tsukita, S., Tsukita, S., and Hakoshima, T. (2003) Structural basis of adhesion-molecule recognition by ERM proteins revealed by the crystal structure of the radixin—ICAM-2 complex. *EMBO J. 22*, 502−514.

DOI: 10.1021/acs.biochem.9b00541
Biochemistry 2019, 58, 3767−3776